Repulsion of polarized particles from two-dimensional materials

Francisco J. Rodríguez-Fortuño, Michela F. Picardi, and Anatoly V. Zayats
Department of Physics, King's College London, Strand, London WC2R 2LS, United Kingdom

(Received 12 July 2017; published 1 May 2018)

Repulsion of nanoparticles, molecules, and atoms from surfaces can have important applications in nanomechanical devices, microfluidics, optical manipulation, and atom optics. Here, through the solution of a classical scattering problem, we show that a dipole source oscillating at a frequency ω can experience a robust and strong repulsive force when its near-field interacts with a two-dimensional material. As an example, the case of graphene is considered, showing that a broad bandwidth of repulsion can be obtained at frequencies for which propagation of plasmon modes is allowed $0 < \hbar\omega < (5/3)\mu_c$, where μ_c is the chemical potential tunable electrically or by chemical doping.

DOI: 10.1103/PhysRevB.97.205401

I. INTRODUCTION

Since the confirmation that light carries momentum in the early 20th century, the study of the mechanical force that light exerts on matter has developed into important scientific and technological applications [1,2]. A simple example of optical force occurs when polarized particles are attracted to a nearby surface: any material surface brought close to an oscillating dipolar particle will experience oscillations of its constituent charges, whose scattered fields then exert forces back on the polarized particle. Under the quasistatic approximation, this is typically explained by an effective image dipole induced in the material [3]. This force can be very strong in the near field and is usually attractive for conventional materials: its influence is behind the unwanted adhesion and stiction in nanomechanical devices [4,5]. Interestingly, recent works show that the surface material's optical properties can turn this attraction into repulsion, even if the particle is in free space [6,7]. The polarized particle can be any source of dipolelike electromagnetic fields, ranging from small illuminated nanoparticles, single atoms, and quantum dot emitters, to radio-frequency dipole antennas. This repulsion of polarized particles from surfaces could lead to interesting novel applications, providing a simple route for levitation of particles or atoms away from a neighboring surface by relying on the optical properties of a surface, instead of requiring structured illumination.

Previous works achieved repulsion of a particle from a surface by using materials whose electric permittivity is near zero [6]. These materials allow no electric field perpendicular to their boundary, intuitively squeezing the electric field between the dipole and the surface, resulting in repulsion [6]. This property is available in natural materials only in narrow frequency bands, and is difficult to synthetize artificially [8,9]. The use of anisotropic materials in which only one of the components of the permittivity tensor is near zero [7] can facilitate realization while retaining the repulsive behavior, but it is still challenging, as finely adjusted thicknesses of metal and dielectric layers are needed to achieve the repulsion in a required spectral range. Even then, the effect is inherently narrowband due to physical constraints: any frequency at which the permittivity is zero must be a point of high dispersion. A similar repulsion was proposed via the use of magneto-optical materials, with a limited bandwidth and requiring external magnets [10].

In this work, we present a simpler mechanism to achieve the repulsion of polarized particles from surfaces. We consider a dipole near a dielectric substrate: any low index dielectric such as glass would work, even if it is nondispersive. The force on a dipole is normally attractive towards such substrate. However, we show that by placing a layer of a two-dimensional (2D) material (such as graphene) on top of this substrate, the force on the dipole becomes repulsive above a certain threshold distance. This repulsive force occurs thanks to the excitation of electromagnetic modes in the 2D layer, a completely different physical effect to the permittivity-near-zero repulsion described above. In addition, the repulsion exists at all frequencies for which such modes exist, which for instance in graphene occurs in a wide range of photon energies lower than graphene's chemical potential, resulting in a huge bandwidth. Two-dimensional materials have been lately shown to have truly remarkable properties, very different to bulk materials, and several practical examples of 2D materials such as graphene, transition metal dichalcogenides (TMDC), and boron nitride are being widely used in nanophotonics and optoelectronics [11]. The presented model also applies to topological insulators, whose surface can be regarded as sheet conductivity. The force acting on harmonically oscillating dipoles is intimately related to fluctuation-induced forces on small particles [12] caused by thermal and quantum fluctuations (nonpolar Van der Waals and Casimir-Polder forces), which are a natural extension of the results presented here. The model could explain the experimentally observed unusual wetting characteristics of graphene [13,14] and Van der Waals forces on molecules near TMDCs [15,16].

II. RESULTS AND DISCUSSION

A. Optical force on dipoles above two-dimensional sheets

We consider a dipole source $\mathbf{p} = (p_x, p_y, p_z)$ radiating with a frequency ω at a position $\mathbf{r}_0 = (0,0,h)$ above a two-dimensional sheet conductivity σ_{2D} which spans the plane $z = 0$, sandwiched between a superstrate and substrate with

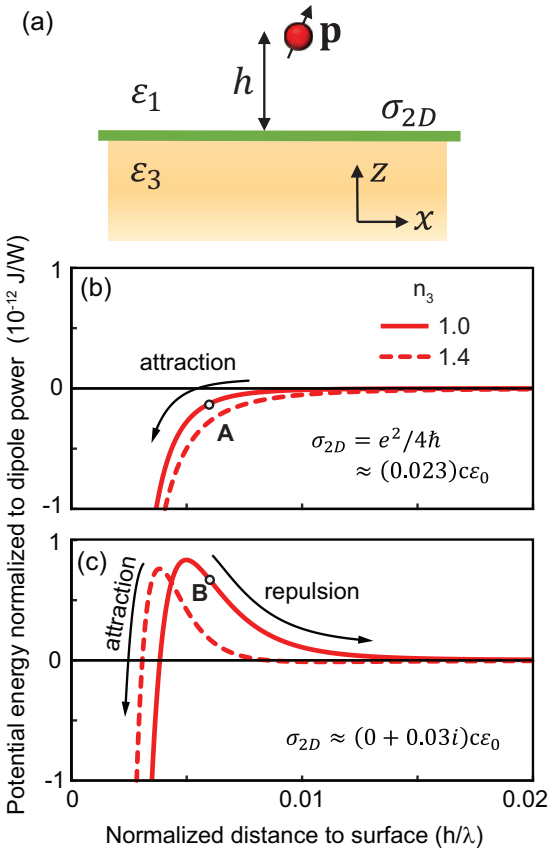

FIG. 1. (a) Geometry of the problem: a dipole **p** radiating at frequency ω (wavelength λ) located a distance h above a 2D material surface on a substrate of relative permittivity ε_3 (refractive index $n_3 = \sqrt{\varepsilon_3}$). The upper medium has relative permittivity $\varepsilon_1 = 1$. (b,c) Numerically calculated potential energy landscape of a horizontally polarized dipole as a function of its distance above the surface, for different values of surface conductivity equal to (b) the ideal conductivity of graphene $\sigma_{2D} = e^2/4\hbar$ (corresponding to label "A" in Figs. 1–3), and (c) a two-dimensional conductivity with a high imaginary part, indicating metallic character (corresponding to label "B" in Figs. 1–3). The refractive index of the substrate is $n_3 = 1$ for solid lines and $n_3 = 1.4$ for the dashed lines The potential energy is normalized to the power radiated by the dipole $P_{\text{rad}} = |\mathbf{p}|^2\omega^4/(12\pi\varepsilon_0\varepsilon_1(c_0^3/n_1^3))$, where $n_1 = \sqrt{\varepsilon_1}$.

respective relative permittivities ε_1 and ε_3 [Fig. 1(a)]. The time-averaged optical force $\langle \mathbf{F} \rangle$ acting on the dipole is given by [17,18]:

$$\langle \mathbf{F} \rangle = \sum_{i=x,y,z} \frac{1}{2} \text{Re}[p_i^* \nabla E_i], \tag{1}$$

where ∇ is the gradient with respect to $\mathbf{r}$ evaluated at $\mathbf{r}_0$, and $\mathbf{E} = (E_x, E_y, E_z)$ is the electric field acting on the dipole reflected back from the surface, which can be calculated following the usual Green's function approach [19,20] (see Appendices A and B for the analytical expression of this force, which depends on materials and geometry). For linearly polarized dipoles, the optical force has no lateral components [21–24] and acts exclusively along z (vertical force). The vertical component $\langle F_z(h) \rangle$ is conservative, allowing us to calculate the potential energy landscape $U(h) = \int \langle F_z \rangle dz$ of the dipole in the vicinity of the surface.

When the dipole is close to a dielectric substrate, the force is attractive. However, a remarkable phenomenon arises when a 2D sheet is placed on top of the substrate: for certain values $h \ll \lambda$, there can be a strong near-field repulsive force acting on the dipole, depending on σ_{2D}. This is the main result of this paper. When the imaginary part of σ_{2D} is close to zero, the potential landscape of the dipole is such that the dipole will be strongly attracted to the surface [Fig. 1(b)]. However, when the values of σ_{2D} have a positive imaginary part, associated with a metallic character of the 2D material enabling it to support plasmon waves, the dipole is then strongly repelled away from the surface if it is beyond a certain threshold distance [Fig. 1(c)]. These values of σ_{2D} are easily achieved in experimental two-dimensional materials as shown below. The repulsion effect is robust to variations in the substrate [Fig. 1(c)], as long as its refractive index is moderately low (e.g., glass). This makes the present system extremely easy to fabricate: given the commercial availability of two-dimensional materials, placing one, such as graphene, over a glass substrate is simple. It is worth noting that if the refractive index of the substrate becomes too high (see Appendix E) the repulsion effect eventually disappears. Therefore the refractive index can be used as a way to tune the repulsive force.

This behavior is very different to previous works on dipole repulsion above semi-infinite materials. The phenomenon observed in two-dimensional sheets can be interpreted as the limiting case of a slab whose thickness is made progressively smaller (see Appendix G). The force behaves differently from the previously studied repulsion of dipoles above permittivity-near-zero surfaces, where the force showed a simple h^{-4} decay with distance under the quasistatic approximation [6,7]. In the present case, the quasistatic limit predicts an attractive force when $h \to 0$ but, crucially; the force undergoes a change of sign in the near field, switching to being repulsive above a threshold distance, corresponding to the local energy maxima in Fig. 1(c). This suggests the presence of competing near-field phenomena. In Fig. 2(a), we plot the dependence of the threshold distance of repulsion, i.e. the contour at which $\langle F_z(z) \rangle$ changes sign for different values of h, as a function of the complex conductivity of the surface σ_{2D}. These contours enclose the regions of σ_{2D} where repulsion occurs for various distances. From a macroscopic optics point of view, ignoring the atomic details, the only relevant optical parameter of a two-dimensional sheet is its complex sheet conductivity σ_{2D} at a certain frequency. Fig. 2 provides a general recipe to the existence of repulsion from two-dimensional sheets at any given distance. Figure 2(b) plots the magnitude of the repulsive force at a fixed distance $h = 0.006\lambda$, constituting a zoomed cross-section of Fig. 2(a).

B. Optical forces on dipoles above graphene

As a practical example of the ideas above, we will consider the behavior of graphene. We would like to stress that all the above results are general and apply to any 2D material, and we only choose graphene as an example due to its well-characterized optical properties. The simplest ideal model for graphene is given by the conductivity $\sigma_{2D} = e^2/4\hbar \approx$

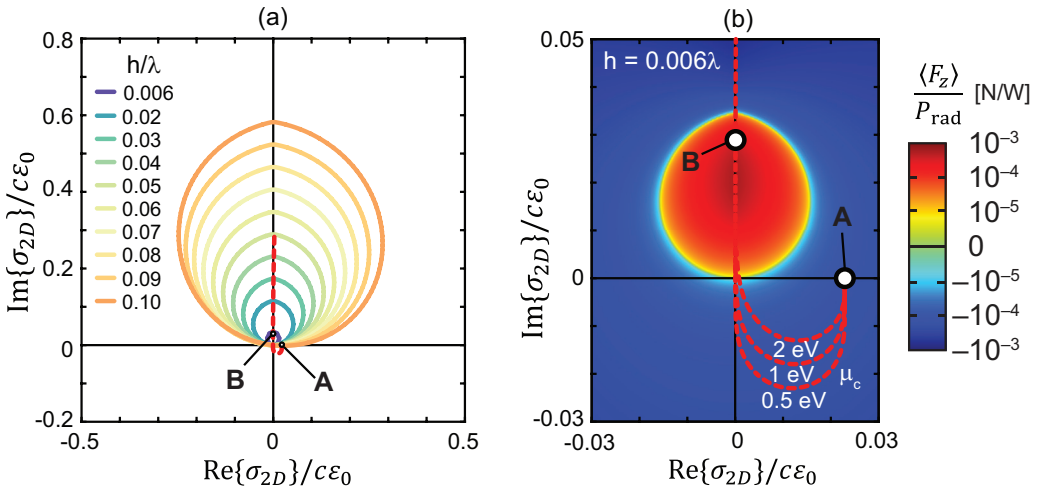

FIG. 2. (a) Contour plot in the complex plane of graphene conductivity σ_{2D} enclosing the region of conductivity for which a repulsive force takes place, for different dipole heights. (b) Time-averaged vertical force acting on the dipole plotted in the complex plane of σ_{2D} [zoom-in from (a)] for a fixed height $h = 0.006\lambda$. (Dashed red lines) parametric plot of the conductivity of graphene as the frequency is varied, for graphene with different chemical potentials obtained from the Kubo formula. The conductivity of ideal graphene is labelled "A," which coincides with the limit of Kubo formula at high frequencies $\hbar\omega \gg \mu_c$. The conductivity for graphene with a chemical potential μ_c at a certain frequency, arbitrarily chosen for strong repulsion in a region of metallic character, is labelled as "B." The conductivity of graphene for different values of μ_c crosses point "B" at different frequencies (e.g., for $\mu_c = 2\,\mathrm{eV}$, it happens at $\hbar\omega = 1.65\,\mathrm{eV}$). The plots correspond to a horizontally polarized dipole $\mathbf{p} = p_x\hat{\mathbf{x}}$ over a free standing 2D material (taking $\varepsilon_1 = \varepsilon_3 = 1$).

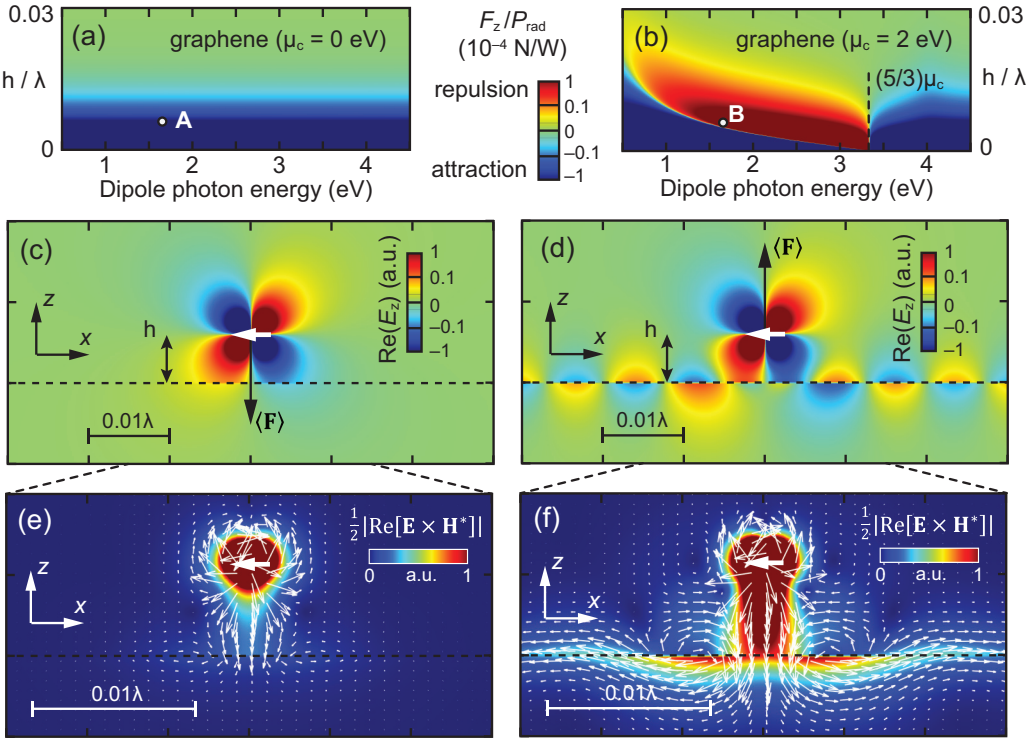

FIG. 3. [(a) and (b)] Parametric map of the optical force acting on a horizontally polarized dipole over graphene as a function of two parameters: the dipole frequency $\hbar\omega$ and the height of the dipole over the surface h. The chemical potential of graphene is set to [(a), (c), and (e)] $\mu_c = 0\,\mathrm{eV}$ (labelled "A" in Figs. 1 and 2) and [(b), (d), and (f)] $\mu_c = 2\,\mathrm{eV}$ (labelled "B" in Figs. 1 and 2). [(c) and (d)] Field plots (z-directed electric field E_z) in the cases "A" and "B," corresponding to attraction and repulsion, respectively, for a dipole height $h = 0.006\lambda$ and a dipole frequency $\hbar\omega = 1.65\,\mathrm{eV}$. [(e) and (f)] Associated time-averaged Pointing vector [zoom-in from (c) and (d)] showing the flux of energy from the dipole into the surface. The fields were calculated by direct integration of the Green functions for the electric and magnetic fields [29]. An exact match of the fields and forces to those from frequency-domain numerical simulations in CST Microwave Studio was confirmed (see Appendix F).

$0.023c\varepsilon_0$. This has zero imaginary part (and, therefore, no repulsion), and is labelled as case "A" in Figs. 1–3. However, graphene exhibits much richer optical phenomena than predicted by this ideal conductivity. The chemical potential μ_c is a well-known characteristic of graphene which can be tuned by chemical doping or by applying an electric bias. When $\mu_c = 0$ eV, graphene's conductivity is given by its idealized value $\sigma_{2D} = e^2/4\hbar$. However, by increasing μ_c, the optical response of graphene can be drastically modified, for instance, allowing the propagation of plasmon modes [25]. Indeed, graphene's conductivity acquires a positive imaginary part at photon energies $\hbar\omega < (5/3)\mu_c$, responsible for its metallic character, and enabling repulsion. The conductivity of graphene $\sigma_{2D}(\omega)$ can be modelled by the widely used Kubo formula known to give good agreement with experiments [25–27] (see Appendix D). The wavelength-dependent conductivity of graphene with different chemical potentials μ_c is shown as red dashed lines on Fig. 2, from which the existence of conductivity values well inside the repulsion region appears clearly. We label an arbitrarily chosen point of the dashed line in this region as case "B" in Figs. 1 –3. This means that the chemical potential of graphene can be used to control and switch the repulsive force that it exerts on a nearby radiating dipole. The frequency-dependent force for a dipole above a graphene layer with chemical potential of $\mu_c = 0$ eV and 2 eV is shown in Figs. 3(a) and 3(b). We see that the repulsion has a very broad bandwidth in the frequency region $0 < \hbar\omega < (5/3)\mu_c$. This observation is confirmed for other values of μ_c, as shown in Appendix E. Figure 3 also shows the associated electric field of the dipole near the graphene layer [Figs. 3(c) and 3(d)] and the time-averaged Poynting vector [Figs. 3(e) and 3(f)]. We can see that the metallic character of graphene (right side of Fig. 3) allows plasmon waves to be excited [28]. We hypothesize that when the dipole energy couples into the surface waves, there is a downward-directed flow of electromagnetic momentum, which must be accompanied by an upwards recoil mechanical force responsible for the repulsion, similar to the mechanism of propulsion in classical mechanics. When the dipole further approaches the surface, repulsion changes into attraction. This is seen in the potential energy landscape from Fig. 1(c) and in the force plot in Fig. 3(b).

C. Forces on illuminated polarizable particles near two-dimensional materials

We now simulate a possible experiment. In the optical regime, a dipolar source is easily realized by the scattering of a small illuminated polarizable particle or molecule. In this case, in addition to the force caused by the dipole scattering itself, the illuminating light will also exert a gradient and scattering force on the particle. This situation can be analyzed as follows: the particle gets polarized by all the fields incident on it, according to $\mathbf{p} = \alpha(\mathbf{E}_{\rm pw}(\mathbf{r}_0) + \mathbf{E}^{\rm r}_{\rm s}(\mathbf{r}_0))$, where α is the isotropic polarizability, $\mathbf{E}_{\rm pw}(\mathbf{r})$ is the superposition of any incident, reflected and transmitted plane waves acting on the scatterer, and $\mathbf{E}^{r}_{\rm s}(\mathbf{r})$ is the back-scattering of the dipole fields reflected from the sheet, which depend on $\mathbf{p}$ and are calculated with the usual Green's function approach. By solving this equation self-consistently for $\mathbf{p}$, we can compute the total time-averaged optical force acting on the particle following Eq. (1) as

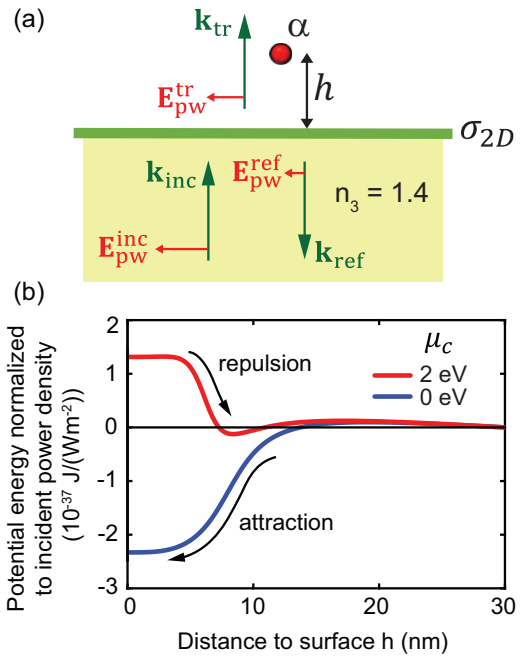

FIG. 4. (a) Point-dipole-like particle near a graphene sheet illuminated under normal incidence from the substrate $n_3 = 1.4$ (through the graphene sheet). (b) Potential energy landscape of a polarizable particle with polarizability $\alpha = (1 + i)(10^{-33})$ m^3 near graphene with chemical potential $\mu_c = 0$ and 2 eV illuminated with light of frequency $\hbar\omega = 1.65$ eV ($\lambda = 750$ nm).

$\langle \mathbf{F} \rangle = (1/2)\sum_{i=x,y,z} \mathrm{Re}\{p_i^* \nabla (E_{{\rm pw},i} + E^{\rm r}_{{\rm s},i})\}$. In this case, the source of energy is the plane wave, and the particle is just a passive scatterer. This removes the infinities that appeared when the dipole was approaching the surface $h \to 0$. Figure 4 shows the potential energy landscape for a polarizable particle near a graphene layer on a glass substrate corresponding to cases "A" ($\mu_c = 0$ eV) and "B" ($\mu_c = 2$ eV), when light is illuminated at normal incidence from below. It clearly shows the switch from attraction to repulsion enabled by the graphene layer. Any other value of nonzero chemical potential can be used for repulsion, as long as the illumination wavelength is chosen in the wide range in which graphene supports plasmons.

III. CONCLUSION

We have shown an extremely simple mechanism for the repulsion of dipoles from a dielectric substrate by the simple addition of conductive two-dimensional sheets. Although we present specific examples for the levitation of polarizable particles over graphene layers with an appropriate chemical potential, the model used in this paper is widely applicable for nano-objects of various sorts, atoms, molecules, particles, emitters, etc., and the results are important in quantum technology, atom optics, microfluidics, and optomechanics.

Our argument relies on the solution of a classical optics scattering problem assuming an ideal dipolar particle and a homogeneous conductivity model for two-dimensional materials, therefore ignoring complexities such as higher-order multipole effects that may arise due to coupling with the surface, as well as the surface atomic arrangements, electronic band structures,

and quantum effects. The fact that such a robust, strong and broadband repulsion arises from this simplest possible model suggests that the result is of fundamental nature, and we expect it to persist in more refined analysis. This is analogous to how repulsion studies for dipoles [6,7] were later found to be extensible to much more complex cases, such as finite-size antennas [30], and even optical repulsion of dielectric waveguides [31].

We did not consider here other sources of forces on the particle, such as electrostatic charging, and fluctuation-induced forces (Casimir-Polder/van der Waals) caused by thermal and quantum fluctuations, which are known to dominate at small distances. In fluctuation electrodynamics, the computation of Casimir interactions can be reduced to solving the classical scattering problem, exactly as performed here, but integrating it over the frequency fluctuations [12]. This leads to an interesting possibility: since the classical scattering repulsion studied in this work exists on a wide frequency range, we expect that fluctuation-induced forces will also be greatly affected. Therefore two-dimensional sheets could have potential for applications in low friction devices [32] by exhibiting reduced attractive or perhaps even repulsive fluctuation-induced forces. This effect could be related with the experimentally observed unusual wetting characteristics of graphene on varying chemical potentials [13,14].

ACKNOWLEDGMENTS

The authors acknowledge helpful discussions with N. Engheta. This work was supported by European Research Council project ERC-2016-STG-714151-PSINFONI and EPSRC (UK). A.Z. acknowledges support from the Royal Society and the Wolfson Foundation. All data supporting this research are provided in full in the text.

APPENDIX A: OPTICAL RESPONSE OF A TWO-DIMENSIONAL SHEET

The Fresnel coefficients of a two-dimensional sheet with sheet conductivity σ_{2D} can be obtained by solving the electromagnetic boundary conditions $\hat{\mathbf{n}} \times (\mathbf{E}_1 - \mathbf{E}_3) = 0$ and $\hat{\mathbf{n}} \times (\mathbf{H}_1 - \mathbf{H}_3) = \mathbf{J}_s$, where $\hat{\mathbf{n}}$ is a unit vector perpendicular to the interface (in this case $\hat{\mathbf{n}} = \hat{\mathbf{z}}$), $\mathbf{E}_1$, $\mathbf{H}_1$, $\mathbf{E}_3$, $\mathbf{H}_3$ are the electric and magnetic fields in the upper and lower media, respectively, and $\mathbf{J}_s = \sigma_{2D}\mathbf{E}_t$ is the surface current density induced in the sheet, proportional to the tangential electric field $\mathbf{E}_t = \mathbf{E}_1 - \mathbf{E}_1 \cdot \hat{\mathbf{n}}$. Alternatively, two-dimensional sheets with a sheet conductivity σ_{2D} can also be modelled as shown in Fig. 5, by considering a slab with a small thickness $\Delta \ll \lambda$, made up of a material with a thickness-dependent effective relative permittivity $\varepsilon_{\text{eff}}(\Delta) = 1 + i\sigma_{2D}/(\omega\varepsilon_0\Delta)$. The optical response of such a thin slab converges, in the limit $\Delta \to 0$, to the behavior of the ideal two-dimensional material with conductivity σ_{2D} [7,25]. Both procedures lead to the complex field transmission and reflection Fresnel coefficients of a two-dimensional sheet sandwiched between materials with relative permittivities ε_1 and ε_3 given by

$$
\begin{aligned}
r^{\text{p}}(k_{\text{t}}) &= \frac{(\varepsilon_3 + k_{z3r}\sigma_{\text{norm}})k_{z1r} - \varepsilon_1 k_{z3r}}{(\varepsilon_3 + k_{z3r}\sigma_{\text{norm}})k_{z1r} + \varepsilon_1 k_{z3r}},\\
t^{\text{p}}(k_{\text{t}}) &= \frac{2(\varepsilon_1\varepsilon_3)^{\frac{1}{2}}k_{z1r}}{\varepsilon_3 k_{z1r} + \varepsilon_1 k_{z3r} + k_{z1r}k_{z3r}\sigma_{\text{norm}}},\\
r^{\text{s}}(k_{\text{t}}) &= \frac{k_{z1r} - (k_{z3r} + \sigma_{\text{norm}})}{k_{z1r} + (k_{z3r} + \sigma_{\text{norm}})},\\
t^{\text{s}}(k_{\text{t}}) &= \frac{2k_{z1r}}{k_{z1r} + k_{z3r} + \sigma_{\text{norm}}},
\end{aligned}
\tag{A1}
$$

where $k_{\text{tr}} = k_{\text{t}}/k_0 = (k_x^2 + k_y^2)/k_0$ is the normalized wave-vector component in the plane parallel to the surface (conserved at the interfaces), $k_{zir} = k_{zi}/k_0 = (\varepsilon_i - k_{\text{tr}}^2)^{1/2}$ is the normalized wave-vector component in the direction perpendicular to the sheet at the ith medium, and $\sigma_{\text{norm}} = \sigma_{2D}/(c\varepsilon_0)$ is a dimensionless way to express the two-dimensional sheet conductivity. The normalization of conductivity and wave-vectors allows Eq. (A1) to be written compactly, and all the quantities involved are dimensionless. The expressions are simplified even further if the substrate and superstrate are equal ($\varepsilon_1 = \varepsilon_3$): for example, $t^p_{\varepsilon_1=\varepsilon_3} = 2\varepsilon_1/(2\varepsilon_1 + k_{zr}\sigma_{\text{norm}})$. Equations (A1) are valid for both propagating ($|k_t| < k_1$) and evanescent ($|k_t| \geqslant k_1$) components, and, therefore, can be used to calculate the fields resulting from any incident field with known spatial Fourier decomposition $E^{p/s}(k_x,k_y)$, including the fields of a dipole source.

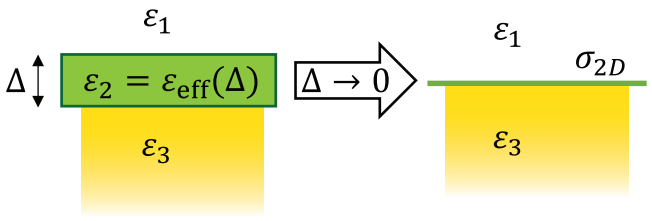

FIG. 5. A two-dimensional sheet with conductivity σ_{2D} can be modeled as a thin slab of thickness Δ with thickness-dependent permittivity $\varepsilon_{\text{eff}}(\Delta) = 1 + i\sigma_{2D}/(\omega\varepsilon_0\Delta)$, whose Fresnel coefficients converge in the limit $\Delta \to 0$.

APPENDIX B: TIME-AVERAGED FORCE ON A DIPOLE NEAR A SURFACE

The time-averaged force vector acting on a dipole near a surface as described in the main text is given by [17,18]

$$
\langle \mathbf{F} \rangle = \sum_{i=x,y,z} \frac{1}{2}\text{Re}\{p_i^* \nabla E_i\},
$$

where ∇ is the gradient with respect to $\mathbf{r}$ evaluated at the location of the dipole $\mathbf{r}_0$, and $\mathbf{E} = (E_x, E_y, E_z)$ is the electric field acting on the dipole (reflected by the surface). To obtain the value of this reflected electric field, we can follow the usual dyadic Green's function approach, in which the field is given by $\mathbf{E}(\mathbf{r}) = \overleftrightarrow{\mathbf{G}}(\mathbf{r},\mathbf{r}_0)\mathbf{p}$. The dyadic Green's function $\overleftrightarrow{\mathbf{G}}$ can be written as a 3×3 matrix which, when multiplied by the dipole vector $\mathbf{p}$, gives us the reflected electric field of a dipole above an arbitrary surface. This Green's function is well-known [19,20] and can be written as a function of the Fresnel reflection coefficients of the surface. Substituting $\mathbf{E}(\mathbf{r}) = \overleftrightarrow{\mathbf{G}}(\mathbf{r},\mathbf{r}_0)\mathbf{p}$ into

the expression of the force, we arrive at

$$\langle \mathbf{F} \rangle = \sum_{i,j=x,y,z} \frac{1}{2}\mathrm{Re}\{p_i^* p_j \nabla G_{ij}\} = \sum_{i,j=x,y,z} \frac{1}{2}\mathrm{Re}\left\{ p_i^* p_j \left(\frac{\partial G_{ij}}{\partial x}\hat{\mathbf{x}} + \frac{\partial G_{ij}}{\partial y}\hat{\mathbf{y}} + \frac{\partial G_{ij}}{\partial z}\hat{\mathbf{z}} \right) \right\}.$$

The summation is done over nine terms, corresponding to the nine elements of each tensor, most of which are zero. Although a lateral force (directed along $\hat{\mathbf{x}}$ or $\hat{\mathbf{y}}$) may exist for circularly polarized dipoles [21–24], corresponding to the terms ∇G_{ij} with $i \neq j$, here we are interested on the vertical force component only, which is given by the terms $\partial G_{ij}/\partial z$

$$\langle F_z \rangle = \langle \mathbf{F} \rangle \cdot \hat{\mathbf{z}} = \sum_{i,j=x,y,z} \frac{1}{2}\mathrm{Re}\left\{ p_i^* p_j \frac{\partial G_{ij}}{\partial z} \right\}.$$

After substitution of the Green's function gradient (see Appendix C), we arrive at the final equation for the vertical force [6,7]:

$$\langle F_z \rangle = \frac{1}{2}\mathrm{Re}\left\{ \frac{-1}{8\pi\varepsilon_0\varepsilon_1} \int_0^\infty k_t \left[(|p_x|^2 + |p_y|^2)\left(k_1^2 r^s - k_{z1}^2 r^p\right) + |p_z|^2 \left(2k_t^2 r^p\right) \right] e^{ik_{z1}2h} dk_t \right\}, \tag{B1}$$

where $k_1 = k_0 n_1 = 2\pi n_1/\lambda_0$ is the wave vector in the upper medium with refractive index n_1 and k_t is the transverse wave vector. The Fresnel reflection coefficients $r^p(k_t)$ and $r^s(k_t)$ of the two-dimensional sheet Eq. (A1) can be substituted into Eq. (B1), which can then be numerically integrated to compute the force. This equation constitutes an exact solution to Maxwell's equations and was used throughout the text for the calculation of the force. The correctness of this expression for the force was carefully confirmed through electromagnetic simulations (see Appendix F and Fig. 8).

APPENDIX C: GREEN FUNCTION'S GRADIENT

The fields reflected by a dipole located at $\mathbf{r}_0$ near a surface defined by $z = 0$ are given in terms of the Green function as $\mathbf{E}(\mathbf{r},\omega) = \overleftrightarrow{\mathbf{G}}(\mathbf{r},\mathbf{r}_0,\omega)\mathbf{p}$. The reflected field Green function for a surface with arbitrary reflection coefficients $r^p(k_t)$ and $r^s(k_t)$ can be written using Weyl's identity [19,20] as

$$\overleftrightarrow{\mathbf{G}}(\mathbf{r},\mathbf{r}_0,\omega) = \frac{i}{8\pi^2\varepsilon_0\varepsilon_1} \iint dk_x dk_y e^{i(k_x(x-x_0)+k_y(y-y_0)+k_{z1}(z+z_0))} \times [r^p \overleftrightarrow{\mathbf{M}}_p + r^s \overleftrightarrow{\mathbf{M}}_s], \tag{C1}$$

where the integral is performed over $k_x, k_y \in [-\infty,\infty]$ and $\overleftrightarrow{\mathbf{M}}_p$ and $\overleftrightarrow{\mathbf{M}}_s$ represent the p- and s-polarized components of the dipole, given by [19]

$$\overleftrightarrow{\mathbf{M}}_p = \begin{pmatrix} -k_{z1}k_x^2/k_t^2 & -k_{z1}k_x k_y/k_t^2 & -k_x \\ -k_{z1}k_x k_y/k_t^2 & -k_{z1}k_y^2/k_t^2 & -k_y \\ k_x & k_y & k_t^2/k_{z1} \end{pmatrix},$$

$$\overleftrightarrow{\mathbf{M}}_s = \frac{k_1^2}{k_{z1}k_t^2} \begin{pmatrix} k_y^2 & -k_x k_y & 0 \\ -k_x k_y & k_x^2 & 0 \\ 0 & 0 & 0 \end{pmatrix}$$

with $k_1 = n_1 k_0 = n_1\omega/c$. The gradient of the Green function with respect to $\mathbf{r} = (x,y,z)$ is given by

$$\nabla \overleftrightarrow{\mathbf{G}} = \frac{\partial \overleftrightarrow{\mathbf{G}}}{\partial x}\hat{\mathbf{x}} + \frac{\partial \overleftrightarrow{\mathbf{G}}}{\partial y}\hat{\mathbf{y}} + \frac{\partial \overleftrightarrow{\mathbf{G}}}{\partial z}\hat{\mathbf{z}},$$

where the spatial derivatives can be directly obtained from Eq. (C1) as

$$\frac{\partial \overleftrightarrow{\mathbf{G}}}{\partial x}(\mathbf{r},\mathbf{r}_0,\omega) = -\frac{1}{8\pi^2\varepsilon_0\varepsilon_1} \iint k_x dk_x dk_y \times e^{i(k_x(x-x_0)+k_y(y-y_0)+k_{z1}(z+z_0))} [r^p \overleftrightarrow{\mathbf{M}}_p + r^s \overleftrightarrow{\mathbf{M}}_s],$$

$$\frac{\partial \overleftrightarrow{\mathbf{G}}}{\partial y}(\mathbf{r},\mathbf{r}_0,\omega) = -\frac{1}{8\pi^2\varepsilon_0\varepsilon_1} \iint k_y dk_x dk_y \times e^{i(k_x(x-x_0)+k_y(y-y_0)+k_{z1}(z+z_0))} [r^p \overleftrightarrow{\mathbf{M}}_p + r^s \overleftrightarrow{\mathbf{M}}_s],$$

$$\frac{\partial \overleftrightarrow{\mathbf{G}}}{\partial z}(\mathbf{r},\mathbf{r}_0,\omega) = -\frac{1}{8\pi^2\varepsilon_0\varepsilon_1} \iint k_{z1} dk_x dk_y \times e^{i(k_x(x-x_0)+k_y(y-y_0)+k_{z1}(z+z_0))} [r^p \overleftrightarrow{\mathbf{M}}_p + r^s \overleftrightarrow{\mathbf{M}}_s].$$

The gradient needs to be calculated at the location of the dipole, therefore, we take the limit $\mathbf{r} \to \mathbf{r}_0$ and assume $\mathbf{r}_0 = (0,0,h)$, which simplifies the expressions to

$$\frac{\partial \overleftrightarrow{\mathbf{G}}}{\partial x}(\mathbf{r}_0,\mathbf{r}_0,\omega) = -\frac{1}{8\pi^2\varepsilon_0\varepsilon_1} \iint k_x dk_x dk_y e^{i2k_{z1}h} \times [r^p \overleftrightarrow{\mathbf{M}}_p + r^s \overleftrightarrow{\mathbf{M}}_s],$$

$$\frac{\partial \overleftrightarrow{\mathbf{G}}}{\partial y}(\mathbf{r}_0,\mathbf{r}_0,\omega) = -\frac{1}{8\pi^2\varepsilon_0\varepsilon_1} \iint k_y dk_x dk_y e^{i2k_{z1}h} \times [r^p \overleftrightarrow{\mathbf{M}}_p + r^s \overleftrightarrow{\mathbf{M}}_s],$$

$$\frac{\partial \overleftrightarrow{\mathbf{G}}}{\partial z}(\mathbf{r}_0,\mathbf{r}_0,\omega) = -\frac{1}{8\pi^2\varepsilon_0\varepsilon_1} \iint k_{z1} dk_x dk_y e^{i2k_{z1}h} \times [r^p \overleftrightarrow{\mathbf{M}}_p + r^s \overleftrightarrow{\mathbf{M}}_s].$$

We can now write the transverse wave vectors in cylindrical coordinates $k_x = k_t \cos\alpha$ and $k_y = k_t \sin\alpha$ and, with some algebra, perform the angular integration in $\alpha \in [0,2\pi]$ leaving

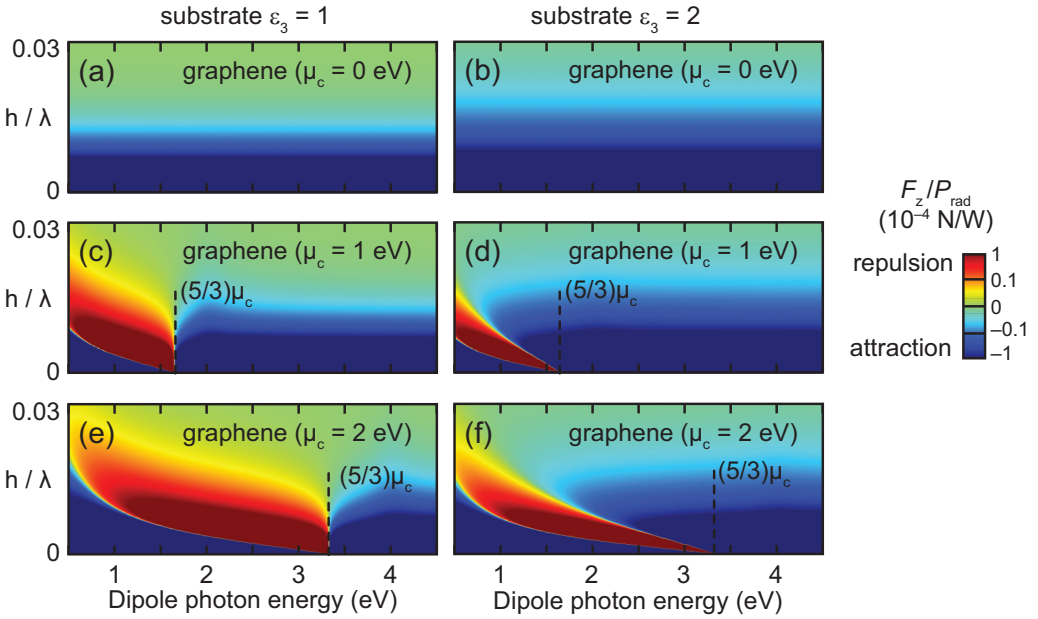

FIG. 6. Map of the vertical force for a vertical dipole over a graphene sheet with different chemical potentials and for different substrate permittivities. The observed behavior is qualitatively identical to a horizontally polarized dipole considered in the main text. The upper frequency limit of the repulsion can be seen to be $(5/3)\mu_c$.

only a single integration over $k_t \in [0,\infty]$:

$$\frac{\partial \overleftrightarrow{\mathbf{G}}}{\partial x}(\mathbf{r}_0,\mathbf{r}_0,\omega) = \frac{1}{8\pi\varepsilon_0\varepsilon_1}\int dk_t e^{i2k_{z1}h}k_t^3 r^p \begin{pmatrix} 0 & 0 & 1 \\ 0 & 0 & 0 \\ -1 & 0 & 0 \end{pmatrix},$$

$$\frac{\partial \overleftrightarrow{\mathbf{G}}}{\partial y}(\mathbf{r}_0,\mathbf{r}_0,\omega) = \frac{1}{8\pi\varepsilon_0\varepsilon_1}\int dk_t e^{i2k_{z1}h}k_t^3 r^p \begin{pmatrix} 0 & 0 & 0 \\ 0 & 0 & 1 \\ 0 & -1 & 0 \end{pmatrix},$$

$$\frac{\partial \overleftrightarrow{\mathbf{G}}}{\partial z}(\mathbf{r}_0,\mathbf{r}_0,\omega) = \frac{1}{8\pi\varepsilon_0\varepsilon_1}\int dk_t e^{i2k_{z1}h}k_t \times \begin{pmatrix} k_{z1}^2 r^p - k_1^2 r^s & 0 & 0 \\ 0 & k_{z1}^2 r^p - k_1^2 r^s & 0 \\ 0 & 0 & -2k_t^2 r^p \end{pmatrix}.$$

These tensors can be substituted in the expression of the force to obtain the final expression for the vertical force given in Eq. (B1). Notice that if the dipole is linearly polarized, we have $p_i^* p_j = p_j^* p_i$, and the lateral components of the force exactly cancel out.

APPENDIX D: KUBO FORMULA FOR THE CONDUCTIVITY OF GRAPHENE

In this work we used the Kubo formula [25–27] to model the conductivity of graphene, which is known to fit well with experimental results. The temperature was taken as $T = 293$ K, the energy gap as 0 eV, and the scattering rate was set at $\Gamma = 1.29$ meV, which is the highest amongst Refs. [25–27]. The results do not depend strongly on the scattering rate.

APPENDIX E: EFFECT OF DIPOLE POLARIZATION AND PRESENCE OF A SUBSTRATE

Figure 6 shows the frequency dependent vertical force acting on a vertical dipole above graphene for different chemical potentials, comparing free standing graphene ($\varepsilon_3 = 1$) with the case of a substrate with $\varepsilon_3 = 2$. By comparison with the figures in the main text, it is clearly seen that the behavior discussed in the main text is robust to changes in dipole polarization and presence of substrate.

Additionally, Fig. 7 shows the same potential energy landscape as the main text Fig. 1(c) but including a whole range of varying refractive index of the substrate between $n_3 = 1$ and 2.5. From both Figs. 6 and 7, we see that as the substrate's refractive index increases, the repulsive region will get smaller and eventually disappear, but the repulsion effects persists for

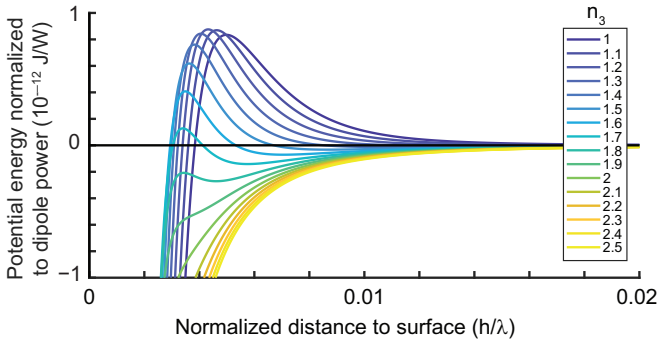

FIG. 7. Numerically calculated potential energy landscape of a horizontally polarized dipole as a function of its distance above the surface, for a two-dimensional conductivity with a high imaginary part and varying refractive index of the substrate. All the other parameters are the same as in Fig. 1(c).

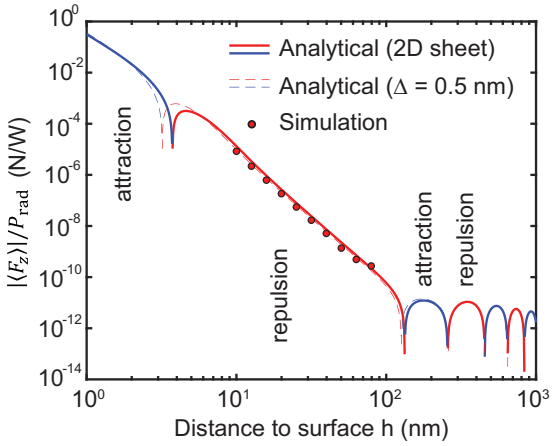

FIG. 8. Logarithmic plot of the distance dependence of the vertical force for a horizontal dipole over a graphene sheet, corresponding to case "B" (frequency $\hbar\omega = 1.65\,\text{eV}$ and graphene chemical potential $\mu_c = 2\,\text{eV}$). Red and blue curves correspond to repulsive and attractive forces, respectively. Comparison between the forces calculated using the numerical integration of Eq. (1) in the main text for graphene modelled as an infinitely thin layer (analytical limit) and as a 0.5-nm-thick layer, and using simulations with CST Microwave Studio in which graphene is modelled as a 0.5-nm-thick layer. In the simulations, the force was obtained from the fields by integration of Maxwell's stress tensor. The force was checked to be independent of the size of the integration volume around the dipole, showing robustness of the result. Numerical noise was relatively large in the last data point due to the very low value of the force.

low index substrates. Interestingly, when $n_3 > 1$, we see that the near field force as a function of distance has two sign changes for a given frequency. This implies a stable point of equilibrium in the potential energy landscape given by a local energy minimum. The equilibrium height depends on the frequency, which suggests interesting applications for particle sorting and manipulation.

APPENDIX F: NUMERICAL SIMULATIONS

The results of the analytical description above were confirmed through the direct solution of full three-dimensional electrodynamic Maxwell's equations for a dipole above a conductive layer, using a commercial electromagnetic simulation software.

Figure 8 shows the comparison between the forces calculated analytically using Eq. (1) and numerically by integrating Maxwell's stress tensor using the commercial software CST Microwave Studio. This simulation requires great care to obtain reliable results, and its details were given in similar simulations performed in Ref. [6].

In the numerical simulations, infinitely thin two-dimensional sheets cannot be modelled. Instead, we modeled graphene as a very thin film of thickness $\Delta = 0.5\,\text{nm}$ with corresponding permittivity $\varepsilon_{\text{eff}}(\Delta)$ as detailed in Fig. 5. In the figure, we also show the analytical calculation of the force for the case of that same thin sheet, seen to give results very close to the infinitely thin sheet. The theory and simulations are in excellent agreement.

APPENDIX G: IMPORTANCE OF THE THICKNESS OF THE MATERIAL

It is a natural question to ask whether the presented effect in 2D materials with a metallic character would also work for slabs of metal with an arbitrary thickness, which also support propagating surface plasmons. In this section, we show that the requirement of such a slab to be thin is fundamental to achieve the broad bandwidth and generality of the repulsion effect: with the 2D material constituting a limiting case.

In a previous study (Ref. [6]), we calculated the force on a dipole above a solid semi-infinite substrate. Repulsion of the dipole is found for those values of the permittivity of the substrate that fulfil the inequality $|\varepsilon| < 1$. This corresponds with an exotic epsilon-near-zero (ENZ) material property, which occurs in metamaterials or in natural materials in very narrow bandwidths. Notice that typical metals are modeled as a negative permittivity (Drude model) at optical frequencies, supporting surface plasmons when $\varepsilon < -1$; even if a metal interface supports surface plasmons for all that range of values of negative permittivity, it does not result in repulsion of dipoles except at its resonance $\varepsilon = -1$, if the losses are low.

However, if one considers a dipole placed above a thin slab of material, then if the material is metallic ($\varepsilon < -1$), we find that the range of values of permittivity for which

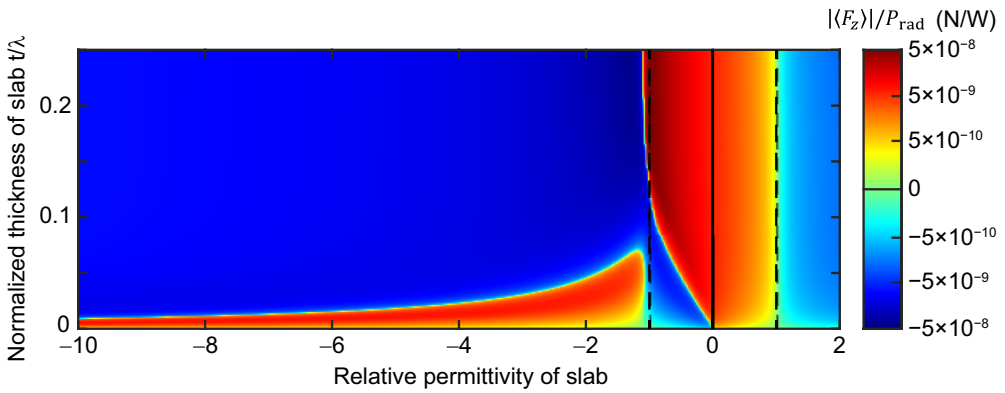

FIG. 9. Vertical force acting on a horizontally polarized dipole placed a distance of 0.1λ above a material slab, as a function of slab thickness and relative permittivity of the slab. The imaginary part of the permittivity was kept constant at 0.1 to add losses.

repulsion exists increases as the thickness of the slab is decreased. This is clearly observed in Fig. 9, calculated using the same equation for the force Eq. (B1) but with the reflection coefficients of a finite slab. The vertical force is plotted as a function of two parameters: the relative permittivity of the slab and the thickness of the slab. For thick slabs ($t > 0.1\lambda$), the behavior quickly tends to the behavior of a solid semi-infinite substrate: only the exotic ENZ values $|\varepsilon| < 1$ result in repulsion. However, there is clearly a limiting case in which, when the thickness of the slab tends to zero ($t \ll \lambda$), the range of permittivities for which repulsion exists varies greatly and in fact increases so as to cover the whole range of permittivities associated with a surface plasmons $\varepsilon < -1$. This suggests the use of the ultimate thin material: a 2D material that behaves as an infinitely thin metal. Indeed, as shown through this work, the 2D material shows repulsion whenever it shows a metallic character. It seems clear from this result that the thickness of the material is fundamental for this effect, and a 2D material is the perfect platform to experimentally achieve ultrathin metal-like layers.

[1] K. Dholakia and T. Čižmár, Nat. Photonics **5**, 335 (2011).
[2] D. G. Grier, Nature (London) **424**, 810 (2003).
[3] J. D. Jackson, *Classical Electrodynamics* (Wiley, New York, NY, 1998).
[4] R. Maboudian and R. T. Howe, J. Vac. Sci. Technol. B Microelectron. Nanom. Struct. **15**, 1 (1997).
[5] N. Tas, T. Sonnenberg, H. Jansen, R. Legtenberg, and M. Elwenspoek, J. Micromech. Microeng. **6**, 385 (1996).
[6] F. J. Rodríguez-Fortuño, A. Vakil, and N. Engheta, Phys. Rev. Lett. **112**, 033902 (2014).
[7] F. J. Rodríguez-Fortuño and A. V. Zayats, Light Sci. Appl. **5**, e16022 (2016).
[8] R. Maas, J. Parsons, N. Engheta, and A. Polman, Nat. Photonics **7**, 907 (2013).
[9] P. Moitra, Y. M. Yang, Z. Anderson, I. I. Kravchenko, D. P. Briggs, and J. Valentine, Nat. Photonics **7**, 791 (2013).
[10] J. A. Girón-Sedas, J. R. Mejía-Salazar, J. C. Granada, and O. N. Oliveira, Phys. Rev. B **94**, 245430 (2016).
[11] F. Xia, H. Wang, D. Xiao, M. Dubey, and A. Ramasubramaniam, Nat. Photonics **8**, 899 (2014).
[12] A. W. Rodriguez, F. Capasso, and S. G. Johnson, Nat. Photonics **5**, 211 (2011).
[13] A. Ashraf, Y. Wu, M. C. Wang, K. Yong, T. Sun, Y. Jing, R. T. Haasch, N. R. Aluru, and S. Nam, Nano Lett. **16**, 4708 (2016).
[14] G. Hong, Y. Han, T. M. Schutzius, Y. Wang, Y. Pan, M. Hu, J. Jie, C. S. Sharma, U. Müller, and D. Poulikakos, Nano Lett. **16**, 4447 (2016).
[15] C. Zhu, Z. Zeng, H. Li, F. Li, C. Fan, and H. Zhang, J. Am. Chem. Soc. **135**, 5998 (2013).
[16] K. Kalantar-zadeh, J. Z. Ou, T. Daeneke, M. S. Strano, M. Pumera, and S. L. Gras, Adv. Funct. Mater. **25**, 5086 (2015).
[17] J. P. Gordon and A. Ashkin, Phys. Rev. A **21**, 1606 (1980).
[18] P. C. Chaumet and M. Nieto-Vesperinas, Opt. Lett. **25**, 1065 (2000).
[19] L. Novotny and B. Hecht, *Principles of Nano-Optics* (Cambridge University Press, New York, 2011).
[20] N. Rotenberg, M. Spasenović, T. L. Krijger, B. le Feber, F. J. García de Abajo, and L. Kuipers, Phys. Rev. Lett. **108**, 127402 (2012).
[21] A. Manjavacas, F. J. Rodríguez-Fortuño, F. J. García de Abajo, and A. V. Zayats, Phys. Rev. Lett. **118**, 133605 (2017).
[22] F. J. Rodríguez-Fortuño, N. Engheta, A. Martínez, and A. V. Zayats, Nat. Commun. **6**, 8799 (2015).
[23] S. Scheel, S. Y. Buhmann, C. Clausen, and P. Schneeweiss, Phys. Rev. A **92**, 043819 (2015).
[24] S. Sukhov, V. Kajorndejnukul, R. R. Naraghi, and A. Dogariu, Nat. Photonics **9**, 809 (2015).
[25] A. Vakil and N. Engheta, Science **332**, 1291 (2011).
[26] G. W. Hanson, J. Appl. Phys. **103**, 064302 (2008).
[27] V. P. Gusynin, S. G. Sharapov, and J. P. Carbotte, J. Phys. Condens. Matter **19**, 026222 (2007).
[28] A. N. Grigorenko, M. Polini, and K. S. Novoselov, Nat. Photonics **6**, 749 (2012).
[29] M. F. Picardi, A. Manjavacas, A. V. Zayats, and F. J. Rodríguez-Fortuño, Phys. Rev. B **95**, 245416 (2017).
[30] S. Krasikov, I. V. Iorsh, A. Shalin, and P. A. Belov, Phys. Status Solidi - Rapid Res. Lett. **8**, 1015 (2014).
[31] M. E. Aryaee Panah, E. S. Semenova, and A. V. Lavrinenko, Sci. Rep. **7**, 3106 (2017).
[32] J. N. Munday, F. Capasso, and V. A. Parsegian, Nature (London) **457**, 170 (2009).